Development of Interatomic Potential for Zr-Ni Amorphous Systems

T. Kumagai*, D. Nikkuni*, S. Hara, S. Izumi and S. Sakai

Mechanical Engineering, School of Engineering, The University of Tokyo, Tokyo 113-861, Japan

This study develops a way of determining the interatomic potential of Zr-Ni using an embedded atom method for binary systems that can reproduce the material properties of its amorphous states. In order to ensure the robustness of the developed interatomic potential, the potential energies and lattice constants of Zr crystals, Ni crystals, and Zr-Ni binary crystals that involve a wide range of local atomic environments are employed for fitting. The elastic properties of some such crystals are also employed. In addition, in order to reproduce Zr-Ni amorphous properties, the radial distribution function of $Zr_{70}Ni_{30}$ amorphous structures and the defect formation energies of Zr-Ni structures are employed. By fitting to a portion of the material properties that requires relatively little computation time, optimization using genetic algorithms is carried out as a first step. As a result, several potential parameter sets are generated. The final potential parameter set, which can reproduce all the material properties used for fitting, is selected from them. The developed potential can reproduce the material properties used for fitting which involve the radial distribution function of the $Zr_{70}Ni_{30}$ amorphous structure.   [doi:10.2320/matertrans.MF200602]

1. Introduction

Amorphous metal shows excellent mechanical properties, such as high tensile strength and large elastic strain.[1] In recent years, amorphous metals that have a stable under-cooled liquid phase have been discovered by Inoue *et al.*[2,3] That such amorphous metals can be obtained at a cooling rate from 0.1 to 100 K/sec allows the fabrication of large-size samples. These amorphous metals are referred to as "metallic glasses". However, the formation mechanism of such metallic glasses remains undetermined. The molecular dynamics (MD) approach is expected to clarify these glass's formation mechanism from an atomic viewpoint.

Two-body interatomic potentials have been used for the MD calculations of amorphous metals since atomic radius and mixing energy can easily be expressed using these potentials.[4,5] However, their applications are limited to qualitative discussions,[4–6] since other material properties such as elastic constants cannot be reproduced. On the other hand, MD calculations employing embedded atom method (EAM) interatomic potentials can reproduce metallic glass more accurately than can those of two-body interatomic potentials,[4,5] since they can reproduce many more material properties than can two-body interatomic potentials. Therefore, EAM interatomic potentials are thought to be suitable for the quantitative description of metallic glass.

Zr-based metallic glasses such as Zr-Ni-Al, Zr-Cu-Al, Zr-Ni-Cu-Al, and Zr-Ti-Ni-Cu-Al systems have high glass forming ability. In order to understand the formation mechanism of such metallic glasses, MD simulations for Zr-Ni amorphous systems can be considered as starting points. Aihara *et al.*[7–12] has investigated Zr-Ni amorphous alloys using Finnis-Sinclar type interatomic potential developed by Massobrio.[13] Although their calculations reproduce various properties of Zr-Ni amorphous structures, quantitative comparisons of structural properties have not been performed. Zhou *et al.* have developed the Generalized EAM (GEAM) interatomic potential, which can deal with Zr-Ni systems.[14,15] Once potential parameter sets for single

component systems have been developed, any combinations of them can be dealt with within the framework of GEAM. However, we have found that the radial distribution function (RDF) of the $Zr_{70}Ni_{30}$ amorphous structure cannot be reproduced by MD calculations employing GEAM interatomic potential.[16] Therefore, the purpose of the present study is to develop an EAM interatomic potential for Zr-Ni binary systems that can reproduce the material properties of Zr-Ni amorphous structures. Among these properties, we pay special attention to the RDF of the material's amorphous structure.

2. The Method for Making Interatomic Potentials

Our method for making interatomic potentials involves the following four processes: 1) detection of a function form, 2) selection and collection of fitting material properties, 3) optimization of potential parameters, and 4) final selection of potential parameter set.[17]

In the "detection of a function form", a suitable potential function form regarding the material's bonding nature (*i.e.*, covalent bonds, metallic bonds, ionic bonds, and mixed bonds) is detected.

In the "material properties used for fitting are selected and collected". Interatomic potentials depend on local atomic environments, such as bond length, bond angle, and coordination number. Therefore, if MD calculation would meet unexpected local atomic environments that were not taken into account in the fitting procedure, the behaviors of the MD system cannot be guaranteed. In addition, a potential should reproduce the key material properties of a particular system in response to the purpose of the study. In order to take into account these two requirements, we propose two types of material properties that are used for fitting. These are referred to as "standard fitting data" and "optional fitting data," respectively.

In order to ensure the robustness of the potential, since interatomic potentials depend on local atomic local environments, energy curves as a function of such local atomic environments should be reproduced. Therefore, basically the basic values of the potential energy of atomic configurations

---

*Graduate Student, The University of Tokyo

that involve a wide range of such local atomic environments should be selected. However, it is difficult to reproduce the energy curves of a part of local atomic environments by fitting them to such material properties directly. In such cases, as an alternative, material properties that describe derivatives of potential energy with respect to a local atomic environment should be selected for fitting. For example, in order to reproduce an energy curve as a function of bond length, potential energy, and bulk modulus at the equilibrium state can be selected. In the present method, these material properties for ensuring robustness are referred to as "standard fitting data."

In order to reproduce key material properties for the purpose of MD calculation, "optional fitting data" are used for fitting.

Only established experimental data are employed as material properties for fitting. Other unestablished data and the material properties of hypothetical configurations are obtained from first principles calculations.

Potential parameters are optimized using a multi-dimensional optimization method. In order to avoid the local minimum problem, potential parameters are optimized using a global-search procedure. Especially, genetic algorithm (GA)[18] is thought to be suitable for optimization of potential parameters, since it is not necessary to calculate the troublesome differentials of potential energy with respect to potential parameters in the fitting procedure. In addition, optimization of potential parameters can be restarted from potential parameter sets obtained from previous optimizations. By fitting to standard fitting data and part of optional fitting data, which takes little computation time, optimization is carried out as a first step. As a result, several potential parameter sets are generated. Optimization function of a potential parameter set is defined as sum of polynomials of differences between material properties used for fitting and those obtained using the potential parameter set:

$$f(\boldsymbol{P}) = \sum_i \sum_j w_{i,j} |\phi_i^{fit} - \phi_i^{\boldsymbol{P}}|^j, \qquad (1)$$

where, $\boldsymbol{P}$ is a potential parameter set, $f(\boldsymbol{P})$ is optimization function for $\boldsymbol{P}$, ϕ_i^{fit} is ith material property used for fitting, $\phi_i^{\boldsymbol{P}}$ is that obtained using $\boldsymbol{P}$ and $w_{i,j}$ is weight of jth power for ith material property used for fitting. $w_{i,j}$ should be adjusted during fitting process.

The potential parameter set, which can reproduce all material properties used for fitting (including standard fitting data and all of optional fitting data), is finally selected from potential parameter sets generated in the optimization of potential parameters process.

3. Development of Zr-Ni Interatomic Potential

3.1 Potential function form

In this study, the interatomic potential function, whose function form is a form of improved GEAM potential function,[14,15] is based on the EAM framework.[19–21] The total energy E of the system is written as eq. (2),

$$E = \frac{1}{2}\sum_i \sum_{j(\neq i)} \phi_{a_i a_j}(r_{ij}) + \sum_i F_{a_i}(\rho_i), \qquad (2)$$

where i and j indicate atomic index, a_i indicates the atomic species of atom i, r_{ij} denotes the interatomic distance between atom i and j, ρ_i denotes the background electron density at atom i, $\phi_{ab}(r)$ is the pair potential function between atomic species a and atomic species b, and $F_a(\rho)$ is the embedding function of atomic species a.

Pair function term $\phi_{ab}(r)$ is defined as eq. (3),

$$\phi_{ab}(r) = f_{\kappa,ab}(r)A_{ab}\exp\left[-\alpha_{ab}\left(\frac{r}{r_{e,ab}}-1\right)\right]$$
$$- f_{\lambda,ab}(r)B_{ab}\exp\left[-\beta_{ab}\left(\frac{r}{r_{e,ab}}-1\right)\right], \qquad (3)$$

where A_{ab}, B_{ab}, α_{ab}, β_{ab}, and $r_{e,ab}$ are potential parameters between atomic species a and b, and $f_{\kappa,ab}(r)$ and $f_{\lambda,ab}(r)$ are cutoff functions between atomic species a and b. This pair function term depends on interatomic distance, the chemical order of the atomic pair, and the number of neighboring atoms (i.e., $\sum_{j(\neq i)}$).

Two cutoff functions $f_{\kappa,ab}(r)$ and $f_{\lambda,ab}(r)$ are defined as eq. (4) and eq. (5), respectively,

$$f_{\kappa,ab}(r) = \begin{cases} 1, & r \leq \kappa_{ab}r_{e,ab} \\ \dfrac{1}{1 + \left(\dfrac{r}{r_{e,ab}} - \kappa_{ab}\right)^{N_{\kappa,ab}}}, & r > \kappa_{ab}r_{e,ab} \end{cases} \qquad (4)$$

$$f_{\lambda,ab}(r) = \begin{cases} 1, & r \leq \lambda_{ab}r_{e,ab} \\ \dfrac{1}{1 + \left(\dfrac{r}{r_{e,ab}} - \lambda_{ab}\right)^{N_{\lambda,ab}}}, & r > \lambda_{ab}r_{e,ab} \end{cases} \qquad (5)$$

where κ_{ab}, λ_{ab}, $N_{\kappa,ab}$, and $N_{\lambda,ab}$ are the potential parameters between atomic species a and b. These forms are similar to those proposed by Zhou et al.[14,15]

The background electron density of atom i, ρ_i, can be defined by the sum of the partial electron densities of the neighboring atoms,

$$\rho_i = \sum_{j(\neq i)} f_{e,a_j a_i} f_{a_j}(r_{ij}), \qquad (6)$$

$$f_a(r) = f_{\lambda,aa}(r)\exp\left[-\beta_{aa}\left(\frac{r}{r_{e,aa}}-1\right)\right]., \qquad (7)$$

where, $f_{e,ab}$ indicates electron density ratio of atomic species a to b. Therefore, the conditions

$$f_{e,aa} = 1, \qquad (8)$$

$$f_{e,ab} = \frac{1}{f_{e,ba}}, \qquad (9)$$

are imposed. This background electron density ρ_i depends on the number of neighboring atoms (i.e., $\sum_{j(\neq i)}$), the atomic species of neighboring atoms (i.e., $f_{e,a_j a_i}$), and the interatomic distances between atom i and neighboring atoms (i.e., $f_{a_j}(r_{ij})$).

By connecting the following three functions (i.e., eq. (10), eq. (11), and eq. (12)), embedding function $F(\rho)$ can be defined as,

$$F_a(\rho) = \sum_{i=0}^{3} F_{n_i,a}\left(\frac{\rho}{\rho_{n,a}} - 1\right)^i, \rho < \rho_{n,a},$$

$$\rho_{n,a} = T_{n,a}\rho_{e,a}, \qquad (10)$$

$$F_a(\rho) = \sum_{i=0}^{3} F_{i,a}\left(\frac{\rho}{\rho_{e,a}} - 1\right)^i, \rho_{n,a} \leq \rho < \rho_{u,a},$$

$$\rho_{u,a} = T_{u,a}\rho_{e,a}, \tag{11}$$

$$F_a(\rho) = F_{e,a}\left[1 - \ln\left\{\left(\frac{\rho}{\rho_{s,a}}\right)^{\eta_a}\right\}\right]\left(\frac{\rho}{\rho_{s,a}}\right)^{\eta_a}, \rho_{u,a} \leq \rho, \tag{12}$$

where, $\rho_{e,a}$, $\rho_{s,a}$, $T_{n,a}$, $T_{u,a}$, η_a, $F_{n_i,a}(i = 0 \sim 3)$, and $F_{i,a}(i = 0 \sim 3)$ are potential parameters for atomic species a. It should be noted that the potential parameters are optimized so that these three functions are continuous at two connection points (*i.e.*, $\rho_{n,a}$ and $\rho_{u,a}$) up to second-order derivatives. These are similar forms to those proposed by Zhou *et al.* However, the restrictions $T_{n,a} = 0.85$ and $T_{u,a} = 1.15$ are eliminated.[14,15]

After all, the potential function can be incorporated with local atomic environments such as interatomic distance, the number neighboring atoms, and chemical order. If the system involves only a single component and the following conditions (eq. (13)) are imposed, the potential function form would be equivalent to the GEAM potential function form,

$$\rho_{e,a} = \frac{\rho_{e,a}^{GEAM}}{f_{e,a}^{GEAM}}, \rho_{s,a} = \frac{\rho_{s,a}^{GEAM}}{f_{e,a}^{GEAM}},$$

$$A_{aa} = A_a^{GEAM}, B_{aa} = B_a^{GEAM},$$

$$\alpha_{aa} = \alpha_a^{GEAM}, \beta_{aa} = \beta_a^{GEAM}, r_{e,aa} = r_{e,a}^{GEAM},$$

$$\kappa_{aa} = \kappa_a^{GEAM}, \lambda_{aa} = \lambda_a^{GEAM}, N_{\kappa,ab} = 20, N_{\lambda,ab} = 20$$

$$f_{e,ab} = \frac{f_{e,a}^{GEAM}}{f_{e,b}^{GEAM}} T_{u,a} = 1.15, T_{n,a} = 0.85, \tag{13}$$

where potential parameters with the superscript *GEAM* denotes the original GEAM potential parameters.

3.2 Selection and collection of fitting material properties
3.2.1 Selection for Zr-Zr and Ni-Ni potential parameters

Since the potential function can be incorporated with interatomic distance and the number of neighboring atoms as a potential function for single component systems, the standard fitting data for these local atomic environments should be selected.

As standard fitting data for the number of neighboring atoms, cohesive energies for DIAMOND Zr, SC Zr, BCC Zr, FCC Zr, HCP Zr, DIAMOND Ni, SC Ni, BCC Ni, FCC Ni, and HCP Ni, as well as their lattice constants are employed. As standard Fitting data for interatomic distance, the elastic constants of FCC Ni and HCP Zr and the bulk moduli of SC Ni, BCC Ni, FCC Ni, SC Zr, BCC Zr, FCC Zr, and HCP Zr are employed. Energy curves as a function of atomic volume are fitted to within the range of 70%–130% around the equilibrium atomic volume for SC Ni, BCC Ni, FCC Ni, BCC Zr, FCC Zr, and HCP Zr as standard fitting data for interatomic distance. In addition, the defect formation energies of FCC Ni and HCP Zr are employed as optional fitting data.

Since the structures of SC Ni, BCC Ni, HCP Ni, SC Zr, BCC Zr, and FCC Zr are hypothetical, the material properties of these structures are obtained from first principles calcu-

Table 1 Coordination numbers of various Zr-Ni binary crystals. Z_{Zr} is total coordination number of atomic species Zr and Z_{ZrNi} is number of atomic species Ni included in Z_{Zr}.

Structure		Coordination Number			
		Z_{ZrZr}/Z_{Zr}	Z_{ZrNi}/Z_{Zr}	Z_{NiNi}/Z_{Ni}	Z_{NiZr}/Z_{Ni}
SC	Zr_7Ni	4/6, 6/6	2/6, 0/6	0/6	6/6
SC	Zr_6Ni_2	4/6	2/6	0/6	6/6
NaCl	$ZrNi$	0/6	6/6	0/6	6/6
SC	Zr_2Ni_6	0/6	6/6	4/6	2/6
SC	$ZrNi_7$	0/6	6/6	4/6, 6/6	2/6, 0/6
BCC	$Zr_{12}Ni_4$	4/8, 8/8	4/8, 0/8	0/8	8/8
BCC	$Zr_{10}Ni_6$	2/8, 8/8	6/8, 0/8	0/8	8/8
CsCl	$ZrNi$	0/8	8/8	0/8	8/8
BCC	Zr_6Ni_{10}	0/8	8/8	2/8, 8/8	6/8, 0/8
BCC	Zr_4Ni_{12}	0/8	8/8	4/8, 8/8	4/8, 0/8
BCC	Zr_2Ni_{14}	0/8	8/8	6/8, 8/8	2/8, 0/8
FCC	Zr_3Ni	8/12	4/12	0/12	12/12
FCC	Zr_2Ni_2	4/12	8/12	4/12	8/12
FCC	$ZrNi_3$	0/12	12/12	8/12	4/12
Cu_2Mg	Zr_2Ni	6/12	6/12	4/16	12/16
Cu_2Mg	$ZrNi_2$	4/16	12/16	6/12	6/12

lations. Energy curves, which cannot be collected from experiments, are also obtained from first principles calculations. Other material properties are collected experimentally.

3.2.2 Selection for Zr-Ni potential parameters

For a binary component system, the potential function can be incorporated with interatomic distance, the number of neighboring atoms, and chemical order. Therefore, the standard fitting data for such local atomic environments should be selected.

Formation energies and lattice constants for SC-type, BCC-type, FCC-type, and Cu_2Mg-type binary systems are employed as standard fitting data for the number of neighboring atoms and their chemical order. Since BCC-type $Zr_{14}Ni_2$ was not converged in the first principles calculations, it is not included in the BCC-type binary systems. SC-type binary systems include SC-type Zr_7Ni, Zr_6Ni_2, NaCl, Zr_2Ni_6, and $ZrNi_7$ as shown in Table 1 and Fig. 1. Energies of SC Zr and SC Ni are selected as reference energies for them. BCC-type binary systems include BCC-type $Zr_{12}Ni_4$, $Zr_{10}Ni_6$, CsCl, Zr_6Ni_{10}, Zr_4Ni_{12}, and Zr_2Ni_{14} as shown in Table 1 and Fig. 1. Energies of BCC Zr and BCC Ni are selected as reference energies for them. FCC binary systems include FCC Zr_3Ni, Zr_2Ni_2, and $ZrNi_3$ as shown in Table 1 and Fig. 1. Energies of FCC Zr and FCC Ni are selected as reference energies for them. Cu_2Mg-type Zr_2Ni, and $ZrNi_2$ as shown in Table 1 and Fig. 1. Energies of HCP Zr and FCC Ni are selected as reference energies for them. Since the cohesive energies of the reference states are not perfectly reproduced by the developed interatomic potentials, formation energies which are relative values are employed for fitting. It is noted that these structures involve a wide range of numbers and chemical order of neighboring atoms as shown in Table 1.

The bulk moduli of FCC-type Zr_3Ni, FCC-type $ZrNi_3$, Cu_2Mg-type Zr_2Ni, and Cu_2Mg-type $ZrNi_2$ are employed as
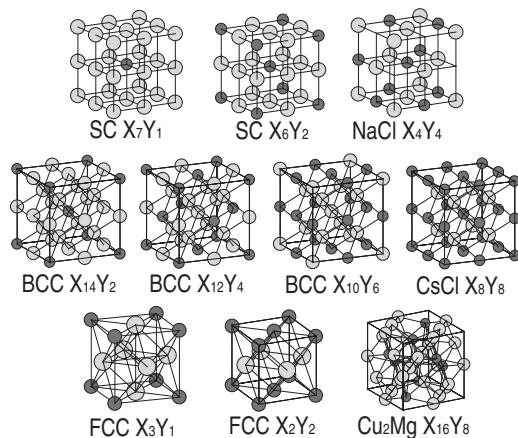
Fig. 1   A schematic figure of the crystal structures used for fitting.

the standard fitting data for interatomic distance and its chemical order.

Since amorphous structures are thought to be similar defected structures, octahedral-type Zr interstitial, octahedral-type Ni interstitial, (100) split-type Zr interstitial near the Zr site (split-type Zr-Zr interstitial), (100) split-type Zr interstitial near the Ni site (split-type Zr-Ni interstitial), (100) split-type Ni interstitial near the Zr site (split-type Ni-Zr interstitial), (100) split-type Ni interstitial near the Ni site (split-type Ni-Ni interstitial), and mono vacancy formation energies for FCC-type Zr_3Ni FCC-type Zr_2Ni_2 FCC-type $ZrNi_3$ are employed as optional fitting data, respectively.

Since the purpose of this study is to reproduce the Zr-Ni amorphous structure, the RDF of the $Zr_{70}Ni_{30}$ amorphous structure is employed as optional fitting data. The lattice constants and formation energies of several stable Zr-Ni alloys[22,23] are also added to the optional fitting data. As candidates of stable Zr-Ni alloys, Al_2Cu-type Zr_2Ni, Zr_2Ni, Fe_2P-type Zr_2Ni, CrB-type ZrNi, Al_2Cu-type $ZrNi_2$, and Fe_2P-type $ZrNi_2$ are employed. The reference energies of these structures are HCP-type Zr and FCC-type Ni. A great deal of time is needed to compute the RDF and material properties of these alloys, which have several structural parameters. Therefore, these material properties are not used for the optimization of potential parameters, and are used only for the selection of the final potential parameter set in the final selection of the potential parameter set.

3.2.3   Collection of fitting material properties

In this study, plane-wave pseudopotential calculations based on density functional theory were performed using the Vienna abinitio simulation package (VASP)[24,25] for first principles calculations. The energy cutoff of the planewave basis was set at 400 eV, and spin polarized generalized gradient approximation (GGA) proposed by Perdew, Berke, and Ernzerhof[26] was employed as a exchange-correlation functional. Monkhorst-Pack k-point grids are used for the k-point sampling.[27] Since the material properties obtained from first principles calculations using the plane wave pseudopotential method based on density functional theory do not accurately agree with those obtained experimentally, they are converted in order to achieve consistency with the experimental material properties. The details of this conversion are described in the Appendix.

The lattice constant of Cu_2Mg-type $ZrNi_2$ (6.916 Å) is collected from the experimental data.[22] The RDF of the $Zr_{70}Ni_{30}$ amorphous structure was collected from the experiment,[28] which was performed using high energy x-ray diffraction of SPring-8 synchrotron radiation. Other material properties are obtained from our first principles calculations.

3.3   Optimization for potential parameters and selection of the final potential parameter set

From sensitivity analysis, $f_{e,ZrNi}$ turned out to greatly affect the shape of RDF. Therefore, we generated many potential parameter sets with respect to various fixed values of $f_{e,ZrNi}$. Other potential parameters are optimized using GA. Among them, we have selected a potential parameter set that best reproduces the RDF of $Zr_{70}Ni_{30}$. As a result, a potential parameter set that involves $f_{e,ZrNi} = 0.215$ is selected. Potential parameter sets that involve $f_{e,ZrNi} > 0.3$ could not reproduce the split first peak of RDF for $Zr_{70}Ni_{30}$ amorphous structures.

In above process, for each optimized potential parameter sets, RDFs of $Zr_{70}Ni_{30}$ amorphous structures were checked. Amorphous structures were fabricated by the melt-quench (MQ) method in the framework of MD simulation. FCC-type structures that involve 350 Zr atoms and 150 Ni atoms were annealed at 5000 K for 0.216 nsec. After that, the system was quenched at the rate of 4×10^{12} K/s. Finally, it was annealed at 500 K for 2.16 nsec.

4.   Results

4.1   Potential parameters

Zr-Zr, Ni-Ni, and Zr-Ni potential parameter sets are shown in Table 2. $\Phi_{ZrZr}(r)$, $\Phi_{NiNi}(r)$, and $\Phi_{ZrNi}(r)$ are shown in Fig. 2.

Two-body functions Φ_{ZrZr}, Φ_{ZrNi}, and Φ_{NiNi}, and partial electron density functions $f_{Zr}(r)$ and $f_{Ni}(r)$ are shown in Fig. 3 and Fig. 4, respectively.

Embedding functions Zr $F_{Zr}(\rho)$ and Ni $F_{Ni}(\rho)$ are shown in Fig. 5 and Fig. 6, respectively.
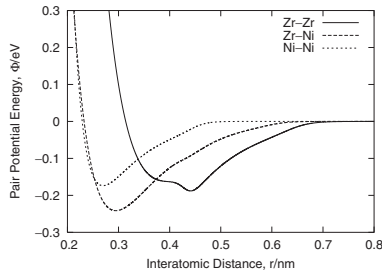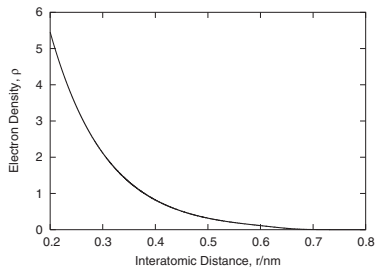
4.2   Material properties for crystals and defected structures used for fitting

The material properties for the crystals and defected structures used for fitting the material properties of HCP-type Zr and FCC-type Ni obtained from the developed interatomic potential are shown in Table 3 and Table 4, respectively. Close agreement with the experimental data was shown.

The relative energies and equilibrium bond lengths of the Zr and Ni polytypes obtained from the developed interatomic potential are shown in Table 5 and Table 6, respectively. The relative energies and equilibrium bond lengths of BCC-type, FCC-type, and HCP-type structures for both Zr and Ni show good agreement with those of GGA, scaled GGA, or experimental data. The relative energies and equilibrium bond lengths of DIAMOND-type and SC structures for both Zr and Ni deviate from GGA, or scaled GGA data. However, these deviations regarding the material properties of DIAMOND and SC structures are thought to be acceptable, since in practice these structures are difficult to realize in bulk due to their high energy states.

Table 2 Optimized potential parameters for Zr-Ni systems.

parameters	Zr-Zr	Ni-Ni	Zr-Ni
f_e	1.00000	1.00000	0.21500
r_e	3.79237	2.32685	2.55111
ρ_e	29.14275	11.18498	—
ρ_s	27.00354	12.30348	—
α	6.74927	9.55109	5.25817
β	3.58856	3.65055	2.94328
A	0.21965	0.41953	0.72302
B	0.37834	0.51023	0.82486
κ	0.14252	0.74640	0.49908
λ	0.71208	0.95262	1.34103
n_κ	39.36483	20.00000	28.47463
n_λ	17.43996	20.00000	31.59732
F_{n0}	−4.48115	−2.88854	—
F_{n1}	−0.23628	−0.03351	—
F_{n2}	1.60210	0.19877	—
F_{n3}	−2.64277	−2.65627	—
F_0	−4.48697	−2.88988	—
F_1	−0.14233	0.00000	—
F_2	1.64714	0.26867	—
F_3	−0.62197	0.17390	—
η	0.71160	0.70541	—
F_e	−4.56219	−2.88266	—
T_n	0.96976	0.92771	—
T_u	1.57419	1.32697	—

Fig. 4 f_{Ni} as a function of interatomic distance.

Fig. 5 F_{Zr} as a function of electron density.

Fig. 6 F_{Ni} as a function of electron density.

Fig. 2 Two-body functions Φ_{ZrZr}, Φ_{ZrNi} and Φ_{NiNi}.

Fig. 3 f_{zr} as a function of interatomic distance.

Table 3 Material Properties for HCP Zr. In this table, a and c indicate the respective lattice constants, E_0 indicates cohesive energy, B indicates bulk modulus, C_{ij} indicates elastic constants, and E_f^v indicates defect formation energy.

	EAM	Exp.[a] (GGA)
a/Å	3.237	3.2312
c/Å	5.149	5.1477
E_0/(eV/atom)	−6.250	−6.25
B/GPa	96.7	96.6 (97.4)
C_{11}/GPa	127.0	144
C_{12}/GPa	68.2	74
C_{13}/GPa	88.4	67
C_{33}/GPa	175.1	166
C_{55}/GPa	29.6	33.4
E_f^v/eV	1.74	1.70

[a]References 31) and references therein

Energy curves as a function of atomic volume obtained from the developed potential of Zr polytypes and Ni polytypes are shown in Fig. 7 and Fig. 8, respectively. In addition, the bulk moduli of the developed potential of the Zr polytypes and Ni polytypes are shown in Table 7. The energy curves and bulk moduli of BCC Zr, FCC Zr, HCP Zr, SC Ni, and FCC Ni show good 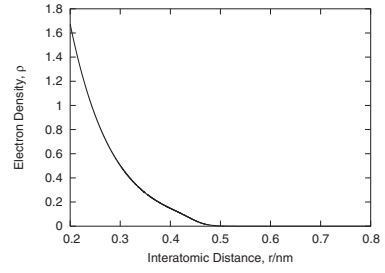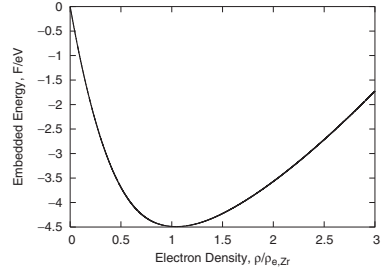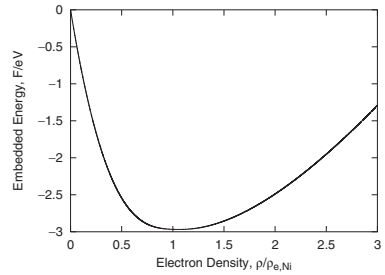agreement with those obtained from GGA. Those of SC Zr deviates from those obtained from GGA. This is thought to be acceptable, since in practice SC Zr is difficult to realize in bulk due to its high energy state. Bulk modulus of BCC Ni also shows deviation from that obtained from GGA. That would be caused by gradually local

Table 4 Material properties for FCC Ni.

	EAM	Exp. (GGA)
$a/\text{Å}$	3.520	3.52[a]
$E_0/(\text{eV/atom})$	−4.440	−4.44[a]
B/GPa	179.4	180.4[b] (200.4)
C_{11}/GPa	243.6	246.5[c]
C_{12}/GPa	147.2	147.3[c]
C_{44}/GPa	128.0	124.7[c]
E_f^v/eV	1.70	1.6[d]

[a]References 32)
[b]is calculated using experimental elastic constants in the reference 33)
[c]References 33)
[d]References 34)

Table 5 Relative energies for Zr and Ni polytypes.

	Relative Energy, $\Delta E/(\text{eV/atom})$			
	Zr		Ni	
crystal	EAM	GGA	EAM	GGA
DIAMOND	1.019	2.310	1.253	2.818
SC	0.462	0.841	0.498	0.692
BCC	0.061	0.078	0.089	0.095
HCP	0	0	0.019	0.023
FCC	0.034	0.040	0	0

Table 6 Lattice constants for Zr and Ni polytypes. In this table, a and c indicate the respective lattice constants.

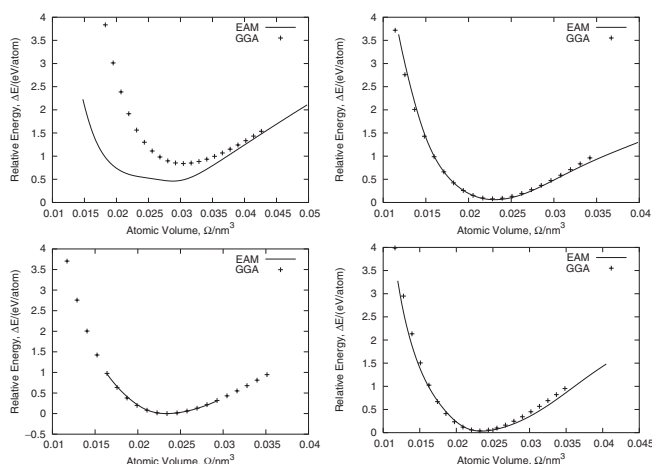|		Lattice Constants, $L/\text{Å}$			
		Zr		Ni	
crystal	axis	EAM	scaled GGA (Exp.)	EAM	scaled GGA (Exp.)
DIAMOND	a	6.245	6.114	5.171	5.100
SC	a	3.066	2.893	2.366	2.329
BCC	a	3.586	3.565	2.805	2.802
HCP	a	3.237	(3.232)[a]	2.484	2.488
	c	5.149	(5.149)[a]	4.107	4.082
FCC	a	4.542	4.519	3.520	(3.52)[b]

[a]References 31) and references therein
[b]References 32)

Fig. 7 Energy curves as a function of atomic volume for Zr polytypes. Upper left shows that of SC Zr, upper right shows that of BCC Zr, lower left shows that of HCP Zr and lower right shows that of FCC Zr.
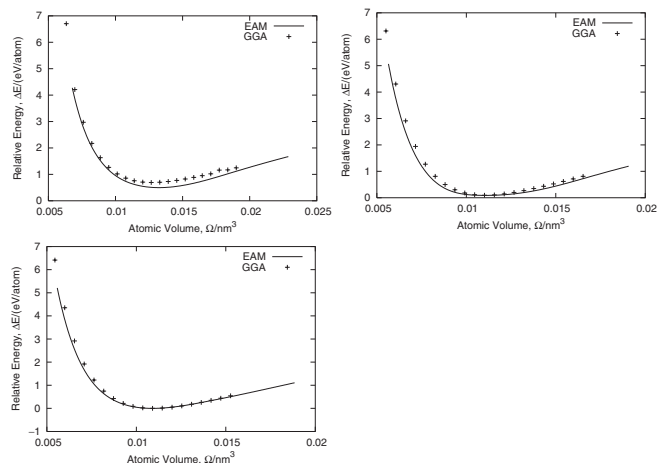

Fig. 8 Energy curves as a function of atomic volume for Ni polytypes. Upper left shows that of SC Ni, upper right shows that of BCC Ni and lower left shows that of FCC Ni.

Table 7 Bulk moduli for Zr and Ni polytypes.

	Bulk Modulus, B/GPa			
	Zr		Ni	
	EAM	Scaled GGA	EAM	Scaled GGA
SC	86.3	65.3	124.1	124.0
BCC	92.4	90.1	80.5	172.1
FCC	87.4	93.7	179.4	180.4
HCP	96.7	96.6	—	—

shape of energy curve around the minimum point. However, this is also thought to be acceptable, since whole shape of energy curve of BCC Ni shows agreement with that obtained from GGA.

The formation energies and lattice constants for Zr-Ni binary crystals obtained from the developed potential are shown in Table 8 and Table 9, respectively. The formation energies of the structures used for fitting can be reproduced to within 0.1 eV/atom of those of GGA except for those of NaCl and Cu_2Mg-type Zr_2Ni. The lattice constants of most structures used for fitting can be reproduced within 3% of those of scaled GGA or experimental data except for those of Al_2Cu-type $ZrNi_2$, Fe_2P-type Zr_2Ni, and CrB-type ZrNi. Since the fitting to RDF of $Zr_{70}Ni_{30}$ amorphous structure is prior to the fitting to other material properties, the order of their energies cannot be reproduced exactly.

The bulk moduli of the Zr-Ni binary crystals used for fitting obtained from MD calculations employing developed interatomic potential are well reproduced, as shown in Table 10.

Defect formation energies used for fitting obtained from the developed interatomic potential are shown in Table 11. These can be reproduced within 1.0 eV/atom of those of GGA except for those of octahedral-type Zr interstitial for FCC-type $ZrNi_3$, octahedral-type Ni interstitial for FCC-type $ZrNi_3$, (100) split-type Zr interstitial near Zr site for FCC-type $ZrNi_3$, and (100) split-type Ni interstitial near Zr site for FCC-type $ZrNi_3$. In this table, in case of $Zr_{25}Ni_8$ and $Zr_{24}Ni_9$, large differences between formation energy of octahedral-type defect and those of split-type defects are shown. In case

Table 8 Reaction Energies of Zr-Ni binary crystals used for fitting.

Crystal	Stoichiometry	Relative Energy, ΔE/(eV/atom)	
		EAM	GGA
SC	Zr_7Ni	−0.033	−0.104
SC	Zr_6Ni_2	−0.233	−0.323
NaCl	Zr_4Ni_4	−0.658	−0.881
SC	Zr_2Ni_6	−0.492	−0.606
SC	$ZrNi_7$	−0.301	−0.246
BCC	$Zr_{12}Ni_4$	−0.189	−0.052
BCC	$Zr_{10}Ni_6$	−0.284	−0.236
BCC	Zr_8Ni_8	−0.465	−0.446
CsCl	Zr_6Ni_{10}	−0.410	−0.343
BCC	Zr_4Ni_{12}	−0.371	−0.381
BCC	Zr_2Ni_{14}	−0.243	−0.163
FCC	Zr_3Ni	−0.104	−0.021
FCC	Zr_2Ni_2	−0.407	−0.379
FCC	$ZrNi_3$	−0.358	−0.440
Cu_2Mg	Zr_2Ni	0.385	0.596
Cu_2Mg	$ZrNi_2$	−0.419	−0.415
Al_2Cu	Zr_2Ni	−0.299	−0.327
Al_2Cu	$ZrNi_2$	−0.212	−0.191
Fe_2P	Zr_2Ni	−0.207	−0.213
Fe_2P	$ZrNi_2$	−0.277	−0.152
CrB	$ZrNi$	−0.352	−0.462

Table 9 Lattice constants of Zr-Ni binary crystals used for fitting. In this table, a, b, and c indicate the respective lattice constants.

crystal	stoichiometry	axis	Lattice Constant, L/Å	
			EAM	Scaled GGA[a] (Exp.)
SC	Zr_7Ni	a	5.620	5.606
SC	Zr_6Ni_2	a	5.431	5.414
NaCl	Zr_4Ni_4	a	5.021	5.188
SC	Zr_2Ni_6	a	4.788	4.833
SC	$ZrNi_7$	a	4.733	4.734
BCC	$Zr_{12}Ni_4$	a	6.729	6.672
BCC	$Zr_{10}Ni_6$	a	6.513	6.527
BCC	Zr_8Ni_8	a	3.157	3.179
CsCl	Zr_6Ni_{10}	a	6.142	6.163
BCC	Zr_4Ni_{12}	a	5.992	5.940
BCC	Zr_2Ni_{14}	a	5.735	5.741
FCC	Zr_3Ni	a	4.334	4.239
FCC	Zr_2Ni_2	a	4.465	4.492
		c	3.157	3.187
FCC	$ZrNi_3$	a	3.642	3.721
Cu_2Mg	Zr_2Ni	a	7.701	7.693
Cu_2Mg	$ZrNi_2$	a	6.950	(6.916)[b]
Al_2Cu	Zr_2Ni	a	6.280	6.447
		c	5.242	5.179
Al_2Cu	$ZrNi_2$	a	4.814	4.978
		c	7.624	7.270
Fe_2P	Zr_2Ni	a	6.605	6.827
		c	4.338	4.156
Fe_2P	$ZrNi_2$	a	7.393	7.356
		c	2.681	2.719
CrB	$ZrNi$	a	3.009	3.267
		b	9.510	9.903
		c	4.329	4.107

[a] All of lattice constants in this table are scaled so that that of Cu_2Mg-type $ZrNi_2$ structure agrees with the experimental one.
[b] References 22) and references therein.

of other interstitial-type defects, the differences are small. This tendency can be reproduced by our developed potential.

In this table, for $Zr_{25}Ni_8$ and $Zr_{24}Ni_9$, differences between formation energy of octahedral-type defect and those of split-type defects are quite large. Our developed potential can reproduce large energy differences for such stoichiometries. Energy differences between them for other stoichiometries are not so large. Our developed potential can also reproduce such energy differences which are not so large.

4.3 Radial distribution function of $Zr_{70}Ni_{30}$ amorphous structure

In the potential fitting process, the $Zr_{70}Ni_{30}$ amorphous structure was fabricated by the MQ method as described in section 3.3. In order to check the RDF of the $Zr_{70}Ni_{30}$ amorphous structure more accurately, the MQ method as performed on a large scale and for a relatively long duration in this section. The result is averaged over 8 cases. The average density turns out to be $7.16\,\mathrm{g/cm^3}$, which is 1.8% larger than that of the data obtained experimentally ($7.03\,\mathrm{g/cm^3}$). The average RDF of $Zr_{70}Ni_{30}$ is shown in Fig. 9, indicating good agreement with the RDF of experimental data, although there exist two deviation points. Those are the appearance of a small shoulder around 4.5 Å, and the position of the third peak around 5.8 Å. However, those are not thought to be so large difference. From the comparison with the result of GEAM potential, the heights of split first peaks have been improved.

5. Discussion

In order to prove the developed potential's applicability to

Table 10 Bulk moduli of Zr-Ni binary crystals used for fitting.

crystal	stoichiometry	Bulk Modulus, B/GPa	
		EAM	Scaled GGA
FCC	Zr_3Ni	95.9	100.0
FCC	$ZrNi_3$	154.4	154.5
Cu_2Mg	Zr_2Ni	79.1	75.4
Cu_2Mg	$ZrNi_2$	143.8	147.2

amorphous states with compositions other than $Zr_{70}Ni_{30}$, $Zr_{36.3}Ni_{63.7}$ amorphous structures were fabricated and compared with experimental data. (As Xu *et al.*[29] pointed out, although Ref. 30) is entitled "Anomalous wide angle x-ray scattering of amorphous Ni_2Zr alloy", the sample was $Zr_{36.3}Ni_{63.7}$.) Partial RDFs (PRDFs) for Zr-Zr, Ni-Zr, and Ni-Ni obtained by x-ray diffraction technique are shown as the experimental data.[30] We calculated experimental RDF using those experimental PRDFs for comparison. The RDF of the $Zr_{36.3}Ni_{63.7}$ amorphous structure is shown in Fig. 10. The RDF obtained from the developed potential shows

Table 11   Defect formation energies of Zr-Ni defected structures used for fitting.

| Original Crystals	Stoichiometry	defect type	defected atom	Defect Formation Energy, E_d^f/(eV/defect)	
				EAM	GGA
FCC-Zr$_3$Ni	Zr$_{25}$Ni$_8$	Octahedral	Zr	4.575	6.114
FCC-Zr$_3$Ni	Zr$_{25}$Ni$_8$	Split	Zr-Zr	4.346	5.143
FCC-Zr$_3$Ni	Zr$_{25}$Ni$_8$	Split	Zr-Ni	−2.192	−1.761
FCC-Zr$_3$Ni	Zr$_{24}$Ni$_9$	Octahedral	Ni	1.043	2.772
FCC-Zr$_3$Ni	Zr$_{24}$Ni$_9$	Split	Ni-Zr	1.263	2.113
FCC-Zr$_3$Ni	Zr$_{24}$Ni$_9$	Split	Ni-Ni	−4.366	−3.995
FCC-Zr$_2$Ni$_2$	Zr$_{17}$Ni$_{16}$	Octahedral	Zr	2.670	3.321
FCC-Zr$_2$Ni$_2$	Zr$_{17}$Ni$_{16}$	Split	Zr-Zr	2.710	2.513
FCC-Zr$_2$Ni$_2$	Zr$_{17}$Ni$_{16}$	Split	Zr-Ni	2.639	3.178
FCC-Zr$_2$Ni$_2$	Zr$_{16}$Ni$_{17}$	Octahedral	Ni	1.130	2.250
FCC-Zr$_2$Ni$_2$	Zr$_{16}$Ni$_{17}$	Split	Ni-Zr	1.263	0.978
FCC-Zr$_2$Ni$_2$	Zr$_{16}$Ni$_{17}$	Split	Ni-Ni	1.174	1.328
FCC-ZrNi$_3$	Zr$_9$Ni$_{24}$	Octahedral	Zr	0.167	0.219
FCC-ZrNi$_3$	Zr$_9$Ni$_{24}$	Split	Zr-Zr	3.206	7.072
FCC-ZrNi$_3$	Zr$_9$Ni$_{24}$	Split	Zr-Ni	0.161	0.232
FCC-ZrNi$_3$	Zr$_8$Ni$_{25}$	Octahedral	Ni	0.946	0.339
FCC-ZrNi$_3$	Zr$_8$Ni$_{25}$	Split	Ni-Zr	2.875	4.408
FCC-ZrNi$_3$	Zr$_8$Ni$_{25}$	Split	Ni-Ni	0.940	0.524
FCC-Zr$_3$Ni	Zr$_{24}$Ni$_7$	Mono Vac	Ni	1.760	2.213
FCC-ZrNi$_3$	Zr$_7$Ni$_{23}$	Mono Vac	Zr	3.100	2.932
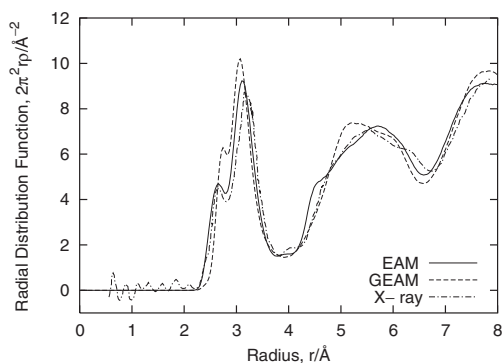
Fig. 9   Radial distribution functions of Zr$_{70}$Ni$_{30}$ amorphous structures. That of experimental data[28] and that obtained using GEAM potential are shown for comparison.
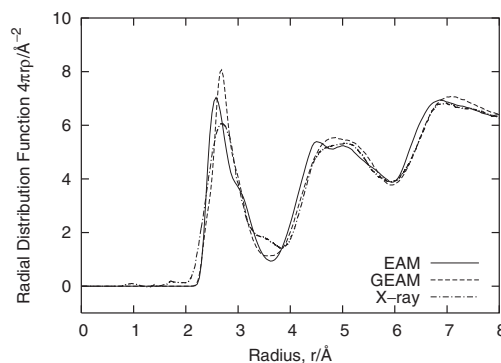

Fig. 10   Radial distribution functions of Zr$_{36.3}$Ni$_{63.7}$ amorphous structure. That of experimental data[30] and that obtained using GEAM potential are shown for comparison.

agreement with that of the experimental data as well as that of GEAM potential except for the sharper first peak and the peak around 4.5 Å. However, since the peak around 4.5 Å is quite larger, the RDF of the Zr$_{36.3}$Ni$_{63.7}$ cannot be reproduced accurately. In order to reproduce that accurately, that is needed to be used for fitting.

6.   Conclusion

In this study, an EAM-type interatomic potential for Zr-Ni binary systems that can reproduce the material properties of Zr-Ni amorphous systems was developed. In order to ensure the robustness of the developed interatomic potential, the potential energies and lattice constants of Zr crystals, Ni crystals, and Zr-Ni binary crystals that involve a wide range of local atomic environments were employed for fitting. In addition, the elastic properties of several Zr crystals, Ni

crystals, and Zr-Ni crystals are also employed. In order to reproduce the Zr-Ni amorphous properties, the RDF of the Zr$_{70}$Ni$_{30}$ amorphous structure and defect formation energies of Zr-Ni structures were employed for fitting. By fitting to the part of the fitting material properties that requires little computation time, optimization was carried out as a first step using GA. As a result, several potential parameter sets were generated. The final potential parameter set, which can reproduce all of the material properties used for fitting, was selected from them. The developed potential can reproduce material properties used for fitting which involve the RDF of the Zr$_{70}$Ni$_{30}$ amorphous structure. In the discussion, applicability of the developed interatomic potential for Zr$_{36.3}$Ni$_{63.7}$ amorphous structure was investigated. RDF of Zr$_{36.3}$Ni$_{63.7}$ amorphous structure was not reproduced accurately. In future, RDFs of other compositions than Zr$_{70}$Ni$_{30}$ are going to be used for fitting.

REFERENCES

1) T. Masuomoto: Science of Machine **40** (1988) 210–214.
2) A. Inoue: Journal of Applied Physics, Japan **67** 1176–1180.
3) A. Inoue: *Progress in Materials Science* **43** (1988) 365–520.
4) M. Shimono and H. Onodera: *Scripta Mater.* **44** (2001) 1595–1598.
5) M. Shimono and H.Onodera: *Materia Japan* **41** (2002) 473–480.
6) M. Shimono and H. Onodera: *Mater. Trans., JIM* **39** (1998) 147–153.
7) T. Aihara, K. Aoki and T. Masumoto: *Scripta Metall. Mater.* **28** (1993) 1003–1008.
8) T. Aihara, K. Aoki and T. Masumoto: *Mat. Sci. Eng. A* **179** (1994) 256–260.
9) T. Aihara, Y. Kawazoe and T. Masumoto: *Mater. Trans., JIM* **36** (1996) 399–407.
10) T. Aihara, Y. Kawazoe and T. Masumoto: *Mater. Trans., JIM* **36** (1996) 835–841.
11) T. Aihara, Y. Kawazoe and T. Masumoto: *Mat. Sci. Eng. B* **37** (1996) 201–204.
12) T. Aihara, Y. Kawazoe and T. Masumoto: *J. Non-cryst. Solids* **37** (1996) 875–878.
13) C. Massobrio, V. Pontikins and G. Martin: *Phys. Rev. B* **41** (1990) 10486–10497.
14) X. W. Zhou, H. N. G. Wadley, R. A. Johnson, D. J. Larson, N. Tabat, A. Cerezo, A. K. Petford-Long, G. D. W. Smith, P. H. Clifton, R. L. Martens and T. F. Kelly: *Acta Mater.* **49** (2001) 4005–4015.
15) X. W. Zhou, R. A. Johnson and H. N. G. Wadley: *Phys. Rev. B* **69** (2004) 144113.
16) D. Nikkuni, T. Kumagai, S. Hara, S. Izumi and S. Sakai: The proceedings of the 11th Symposium on Molecular Dynamics Simulations, (2006) 16–19.
17) T. Kumagai, S. Hara, S. Izumi and S. Sakai: *Modelling and Simulation in Materials Science and Engineering* **14** (2006) S.29–S.37.
18) Kalyanmoy Deb: *Multi-Objective Optimization using Evolutionary Algorithms*, (Wiley, 2001).
19) R. A. Johnson: *Phys. Rev. B* **39** (1989) 12554–12559.
20) M. S. Daw and M. I. Baskes: *Phys. Rev. B* **29** (1984) 6443–6453.
21) Y. Mishin, D. Farkas, M. J. Mehl and D. A. Papaconstantopoulos: *Phys. Rev. B* **59** (1999) 3393–3407.
22) A. E. Carlsson, K. F. Kelton and C. L. Henley: *Phys. Rev. B* **71** (2005) 144103.
23) T. Takeuchi, S. Nakano, M. Hasegawa, K. Soda, H. Sato, U. Mizutani, K. Itoh and T. Fukunaga: *Mater. Trans., JIM* **46** (2005) 2791–2798.
24) G. Kresse and J. Hafner: *Phys. Rev. B* **47** (1993) 558–561.
25) G. Kresse and J. Furthmüller: *Phys. Rev. B* **54** (1996) 11169–11186.
26) J. P. Perdew, K. Burke and M. Ernzerhof: *Phys. Rev. Lett.* **77** (1996) 3865–3868.
27) H. J. Monkhorst and J. D. Pack: *Phys. Rev. B* **13** (1976) 5188–5192.
28) K. Sakai, M. Sakurai, E. Matsubara, T. Ichitsubo, S. Obara and H. Ohsumi: *Abstracts of Spring Meeting of Japan Society of Powder and Powder Metallurgy* (2005), 42.
29) Yan Xu, W. B. Muir, Z. Altounian, W. J. L. Buyers and R. L. Donaberger: *Phys. Rev. B* **53** (1996) 8983–8992.
30) J. C. de Lima, J. M. Tonnerre and D. Raoux: *Journal of non-crystalline solids* **106** (1988) 38–41.
31) W. Hu, B. Zhang, B. Huang, F. Gao and D. J. Bacon: *Journal of Physics: Condensed Mater* **13** (2001) 1193–1213.
32) C. Kittel: *Introduction to Solid State Physics 7th edition*, (John Wiley and Sons, Inc., New York, 1996).
33) G. Simmons and H. Wang: *Single Crystal Elastic Constants and Calculated Aggregate Properties.*, (Cambridge (MA), MIT Press, 1971).
34) W. Wycisk and M. Feller-Kniepmeier: *Journal of Nuclear Materials* **69–70** (1978) 616–619.

Appendix

In order to be consistent with the experimental data, the material properties obtained from first principles calculations need to be converted.

Lattice constants obtained from first principles calculations using the plane wave pseudopotential method employing GGA tend to be overestimated. In order to cancel these overestimations, scaled lattice constants should be used for fitting. The scaling factor is determined so that the scaled lattice constant of the stable structure agrees with those of the experimental data.

Elastic properties of polytype structures except for the stable structure cannot be obtained from experimental data. However, the elastic properties obtained from first principles calculations sometimes deviated from those of the experimental data. Therefore, the scaled bulk modulus is employed for fitting. For a single component system, the bulk modulus of polytype used for fitting B_{poly}^{fit} can be converted as

$$B_{poly}^{fit} = B_{poly}^{FP} \frac{B_{stable}^{Exp}}{B_{stable}^{FP}} \qquad (A\cdot1)$$

where B_{stable}^{Exp} indicates the experimental bulk modulus of the stable structure and B_{poly}^{FP} and B_{stable}^{FP} indicate the bulk modulus of the polytype structure and that of the stable structure obtained from first principles calculations, respectively.

Since the bulk moduli of binary systems used for fitting should be consistent with such scaled bulk moduli of single component systems, those obtained from first principles calculations should be scaled. For P-Q binary systems, the scaled bulk modulus of P_xQ_y, $B_{P_xQ_y}^{fit}$ can be defined as,

$$B_{P_xQ_y}^{fit} = B_{P_xQ_y}^{FP} \frac{xB_P^{pot} + yB_Q^{pot}}{xB_P^{FP} + yB_Q^{FP}}, \qquad (A\cdot2)$$

where $B_{P,ref}^{pot}$ and $B_{Q,ref}^{pot}$ indicate the bulk moduli of P and Q obtained from the developed potential, respectively. $B_{P_xQ_y}^{FP}$, B_P^{FP}, and B_Q^{FP} indicate the bulk modulus of P_xQ_y, P, and Q obtained from first principles calculations, respectively.